Journal of Hazardous Materials 454 (2023) 131553

Contents lists available at ScienceDirect

Journal of Hazardous Materials

journal homepage: www.elsevier.com/locate/jhazmat

Research Paper

Antimony isotope fractionation and the key controls in the soil profiles of an antimony smelting area

Jie Liao [a,b], Decan Tan [a], Haibo Qin [a], Qiao Han [a,b], Enguang Liu [a,b], Jingan Chen [a], Zengping Ning [a,*], Shehong Li [a,*]

[a] State Key Laboratory of Environmental Geochemistry, Institute of Geochemistry, Chinese Academy of Sciences, 550081 Guiyang, China
[b] University of Chinese Academy of Sciences, Beijing 100049, China

HIGHLIGHTS

- Antimony isotopic compositions in soil profiles were measured for the first time.
- Large fractionation of antimony isotopes occurred in the soil profiles.
- Isotope fractionation of natural source Sb may be controlled by plant uptake.
- Smelting source Sb may be controlled by absorption and reductive dissolution.

GRAPHICAL ABSTRACT

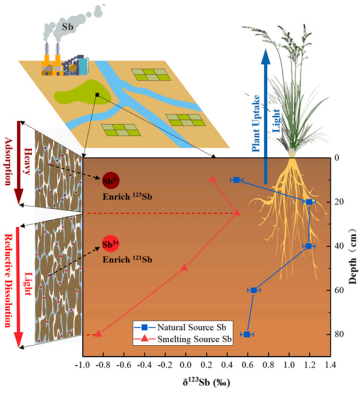

ARTICLE INFO

Editor: Edward Burton

Keywords:
Antimony isotope
Soil profile
Smelting source
Migration and transformation
Fractionation mechanism

ABSTRACT

The controlling factors of antimony migration and transformation in soil profiles are still unclear. Antimony isotopes might be a useful tool to trace it. In this paper, antimony isotopic compositions of plant and smelter-derived samples, and two soil profiles were measured for the first time. The δ^{123}Sb values of the surface and bottom layers of the two soil profiles varied in 0.23‰–1.19‰ and 0.58‰–0.66‰, respectively, while δ^{123}Sb of the smelter-derived samples varied in 0.29‰–0.38‰. The results show that the antimony isotopic compositions in the soil profiles are affected by post-depositional biogeochemical processes. The enrichment and loss of light isotopes at 0–10 cm and 10–40 cm layers of the contrasted soil profile may be controlled by plant uptake process. The loss and enrichment of heavy isotopes in the 0–10 cm and 10–25 cm layers of the antimony from smelting source in the polluted soil profile may be controlled by the adsorption process, while the enrichment of light isotopes in the 25–80 cm layer may be related to the reductive dissolution process. The conclusion emphasizes that the promotion of the Sb isotope fractionation mechanism will play a crucial role in understanding the migration and transformation behaviors of Sb in soil systems.

* Corresponding authors.
E-mail addresses: ningzengping@mail.gyig.ac.cn (Z. Ning), lishehong@vip.gyig.ac.cn (S. Li).

https://doi.org/10.1016/j.jhazmat.2023.131553
Received 11 February 2023; Received in revised form 10 April 2023; Accepted 30 April 2023
Available online 2 May 2023

1. Introduction

Antimony (Sb) is a toxic and carcinogenic metal element, and excessive intake can cause liver dysfunction, skin keratinization, DNA damage, and other problems [5,8,71]. It has been listed as a priority pollutant by the US EPA and the European Union since 1979 [20]. In recent years, studies of peat bogs and Arctic ice cores have shown that Sb is a global pollutant that can travel over long distances [32,50]. At present, as the ninth most mined metal [24], Sb has been widely used, such as flame retardants, antimony lead alloys, lead acid battery electrodes, and antimony chalcogenide solar cells [22,33,51,70].

The concentration of Sb in soil is low, often approximately 1 mg/kg [1]. However, in the antimony mineralized district, the content of Sb in the soil will increase significantly due to the weathering of Sb-rich parent rocks. In addition, with the increase in mining and smelting activities, Sb in soil will further increase, reaching up to 5045 mg/kg [23]. The migration and transformation of Sb in soil are controlled by various biogeochemical processes. Under anaerobic conditions, the reductive dissolution of Fe and Mn (hydro)oxides will cause the release of Sb from Sb-bearing minerals [42,56,21,47]. Sb can also be fixed by the formation of secondary minerals such as Schafarzikite ($FeSb_2O_4$) or coprecipitation with S^{2-} [68]. Under aerobic conditions, the oxidation of Fe(II) minerals will form Fe-containing secondary minerals, causing Sb to coprecipitate with the newly formed secondary minerals [10,29]. Meanwhile, the oxidative dissolution of sulfide will lead to the release of Sb in Sb sulfide [58]. Changes in soil pH due to redox conditions also significantly affect the speciation and migration of Sb. Therefore, it is particularly important to evaluate the contribution of different biogeochemical processes to the overall migration of Sb.

Since the 1990 s, with the rapid development of multi-colletor inductively coupled plasma mass spectrometry (MC-ICP—MS), high-precision metal stable isotopes (such as Fe, Cu, Zn, Cd, Sb, etc.) analysis has been realized, making the tracing of metal stable isotopes for source and process (such as weathering, biomethylation, microbial uptake, redox, etc.) widely used [12,52,63,6,30,66]. It has been proven that the migration and transformation processes of the elements (Fe, Zn, Tl, Cu, etc.) in the soil profile can be traced by the isotopic compositions [67,28,27,31,61].

Sb has two stable isotopes, ^{121}Sb (57.21%) and ^{123}Sb (42.79%) [4]. Sb isotopic compositions of different geological and environmental samples (Fig. 1) indicate that there may be different degrees of isotope fractionation in the biogeochemical processes of Sb in the supergene environment [64], such as reduction, biomethylation, adsorption and other processes [49,62,2]. Tanimizu et al. determined the antimony isotopic composition of the ore and pit water of the Ichinokawa mine in Japan and suggested that the adsorption process can cause isotopic fractionation [55]. Zhai et al. used antimony isotopes to fingerprint hydrothermal fluid flow directionality [72]. Resongles et al. applied antimony isotopes to trace antimony sources in the surface water system of a mining area in France and calculated the Sb contribution ratio of tributaries to the mainstream through a simple mixing model [48]. Therefore, antimony isotopes have the potential to trace the sources and biogeochemical processes in environmental systems [18,72].

At present, research on the speciation and migration behaviors of Sb in the soil is mainly carried out on polluted soil located in the proximity of mines, smelters, and shooting ranges, and there are few studies on

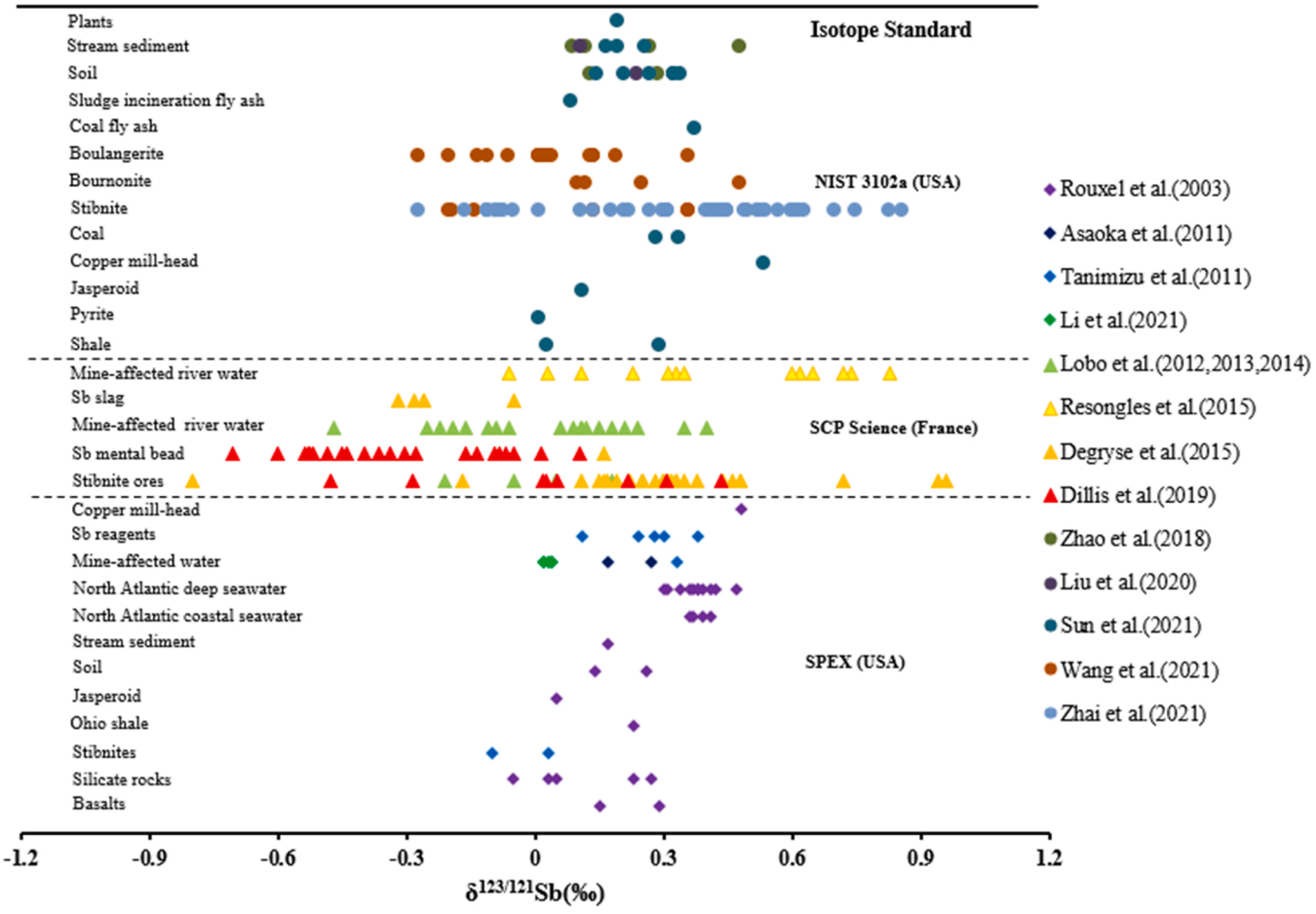

Fig. 1. Antimony isotopic composition of samples from different environmental, geological, and anthropogenic sources [49,3,55,35,40,39,38,48,13,14,73,37,53,59,72].

naturally formed soil. The species and migration pathways of Sb from natural sources in soil may be different from those from pollution sources [19,21]. In addition, there are relatively few comparative studies on the migration and transformation behaviors of anthropogenic and natural sources of Sb in soil profiles. However, such comparative studies will help to understand the differences in controlling the migration and transformation behaviors of anthropogenic and natural sources of Sb in soil, form a more general understanding of the biogeochemical cycle of Sb in soil, and help design more reasonable remediation approaches and methods [28,63].

At present, almost no antimony isotope data in soil systems have been reported. This study is the first to analyze the antimony isotopic composition in contrasted and polluted soil profiles in a high-antimony geological background area. The aim is to 1) verify antimony isotope fractionation in soil profiles; 2) discuss the difference of antimony migration and transformation behavior between contrasted and polluted soil profiles by comparing the antimony isotopic composition characteristics of two soil profiles near and away from the smelting source, combined with the Sb concentration and sequential extraction procedures(SEPs) results; and 3) evaluate the main factors controlling antimony isotope fractionation in the soil system, thus promote the establishment of the theoretical system of antimony isotope fractionation.

2. Sample

2.1. Study area

The sampling sites are located in the southwest of the antimony ore district in Dushan County, Qiannan Buyi and Miao Autonomous Prefecture, Guizhou Province, China. Abundant antimony deposits and occurrences are distributed in the Devonian strata, which are composed of terrigenous clastic rocks and carbonate rocks [41]. New and abandoned antimony smelters are located in this area. The abandoned one was built in 1973 and had a smelting history of more than 40 years, while the new one started operation in 2015 (Fig. 2). The study area has a mid-subtropical warm and humid monsoon climate with an annual precipitation of 1346 mm, the maximum precipitation occurs in July and August, the annual average temperature is 15 °C, the prevailing wind direction is southeasterly (43% frequency), and the average wind speed is 2.4 $m \cdot s^{-1}$ [45].

2.2. Sample collection

The two soil profiles were collected from grassland at different distances from the smelter. Contrasted soil profile S1 was collected approximately 2 km away from the smelter in December 2013, perpendicular to the prevailing wind direction. Due to the relatively high altitude, the soil water holding capacity is poor, and the vegetation is sparse. Polluted soil profile S2 was collected in October 2016 near the smelter. Due to the relatively low altitude and near the river, the vegetation is lush. As both soil profiles are not well stratified vertically, soil was sampled every 10–30 cm. Smelter-derived samples were collected from the smelter. Harvested plant samples (rice and corn) were directly collected from the local farmers. After being brought back to the laboratory, the soil samples were naturally air-dried in a place away from sunlight. The air-dried samples were first passed through a 2 mm sieve, and the sieved part was ground in an agate mortar and then passed through a 200-mesh (<74 μm) sieve. The sieved part was stored in polyethylene bag and then placed separately in kraft paper sample bags

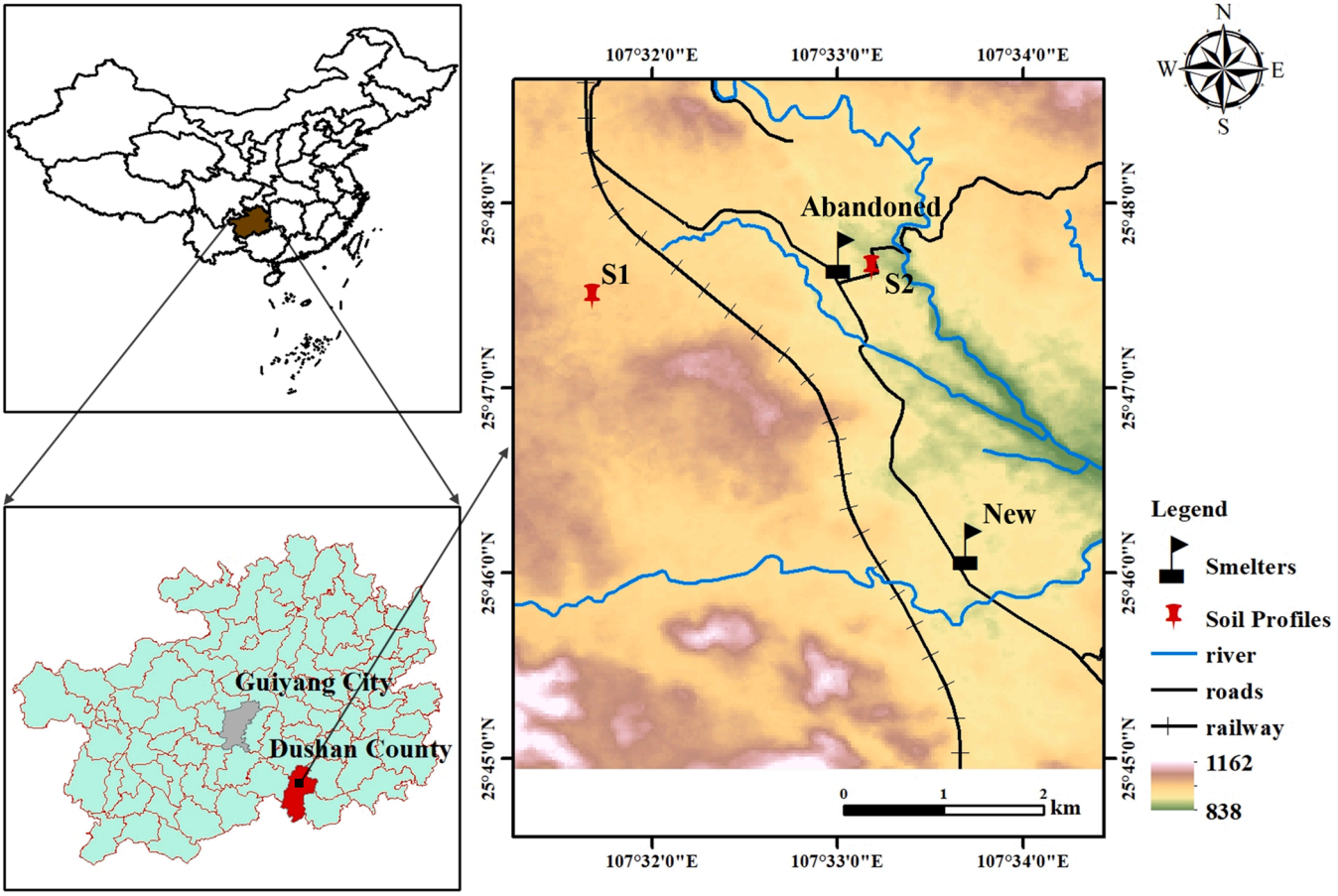

Fig. 2. Overview of the study area and distribution of soil profiles.

for storage. Crushed smelter-derived samples were treated with the same steps as the soil. The plant samples were dried in an oven at 60 °C. Dehulled rice and corn samples were pulverized and then passed through a 60-mesh sieve, and the sieved part was stored in polyethylene bags for digestion. According to the requirements for antimony isotope analysis, two plant samples with relatively high Sb contents were selected for the determination of antimony isotopic composition.

3. Analysis

3.1. Materials and reagents

HNO_3, HCl and HF from the Beijing Institute of Chemical Reagents (China) used in the experiment were subject to secondary distillation by a sub-boiling acid system. H_2O_2 (35%, wt./wt., guarantee reagent grade), $NaBH_4$ (99%), Analytical reagent grade L(+)-Ascorbic acid, Sodium hydroxide (pellets, 98% purity) and 1.0 N Sodium hydroxide (Accurate Standard Volumetric Solution) were obtained from Thermo Fisher Scientific (USA). Potassium iodide (ACS reagent, ≥99%) was from Alfa Aesar. The experimental water (18.2 MΩ cm^{-1}) was prepared by a Milli-Q ultrapure water system. The Sb isotope analysis results of this study were reported against NIST SRM 3102a, High-purity Sb solution from Alfa Aesar (USA) was used as the secondary standard solutions. The cation exchange resin AG50W-X8 (100–200 mesh) and Silica-based thiol resin (Cleanert SH, pore size: 60 Å, grain size: 40 μm) were bought from Bio-Rad Company (USA) and Tianjin Agela Technologies company (China), respectively [11]. The Savillex™ PFA (15 ml) beakers were sequentially cleaned with HNO_3 (1:1), HCl (1:1) and MQ water before use. And pipette tips can refer to the published article [54].

Soil and sediment reference materials GSS-5, GSD-3, GSD-10 and GSD-11 were from the Institute of Geophysical and Geochemical Exploration of the Chinese Academy of Geological Sciences, whereas 2711a(soil) were purchased from NIST.

3.2. Sample digestion

Sample digestion followed procedures described in the published articles [54,74]. The HF-HNO_3 mixed acid system and H_2O_2 was used for total digestion. 1 ml HNO_3 (15.8 M) was added to each Teflon (PTFE) liner vial, and then 50 mg smelter-derived sample, 100 mg soil and 200 mg plant sample powders were weighed into those vials, respectively. Samples were sealed in high-pressure bombs and placed in an oven (185 °C) for at least 36–48 h. After cooling, the vials were heated on a hot plate (temperature should not exceed 90 °C) to evaporate the sample solution to incipient dryness. Finally, the samples were dissolved and stored in 1 ml of 2 M HNO_3 for Sb purification.

3.3. Sequential extraction procedures

To evaluate the mobility of Sb in soil, the modified sequential extraction procedures (SEPs) proposed by [65] were used. This method was originally developed for arsenic (As) and is also widely used for Sb because Sb and As are adjacent periodic elements of the same main group and have similar chemical properties [15,44]. First, 1 g of each soil powder sample was taken into a 50 ml centrifuge tube, and then 25 ml 0.05 M $(NH_4)_2SO_4$ was added and shaken at 200 rpm for 4 h at 25 °C. After centrifugation, non-specifically adsorbed Sb (F1) was obtained; then, 25 ml 0.05 M $NH_4H_2PO_4$ was added to the same sample, which was shaken at 200 rpm for 4 h at 25 °C to extract the non-specifically adsorbed Sb (F2). The residual fraction (F3) was obtained by subtracting the first two fractions from the total concentration. Centrifugation conditions were 4000 rpm for 20 min, and the supernatant was stored for analysis. F1 and F2 together represent the easily migrated Sb in soil. Data quality was controlled by soil standard material, replicate samples, and method blanks.

3.4. Total organic carbon and antimony concentration

Total organic carbon (TOC) was determined by an elemental analyser (vario MACRO cube, Elementar, Germany) [60]. Before analysis, samples were treated with 1 M HCl to remove inorganic carbon. The total Sb and trace element concentrations in soil and plant samples were determined using an atomic fluorescence spectrometer (AFS-920, Beijing Jitian Instrument Co., Ltd.) and inductively coupled plasma mass spectrometry (PlasmaQuant-MS Elite, Jena Analytical Instruments AG, Germany), respectively [36].

3.5. Antimony isotopes analysis

Sample purification for Sb isotope analysis was carried out in a class 100 ultra-clean room of the Institute of Geochemistry, Chinese Academy of Sciences using AG50W-X8 cation exchange resin (100–200 mesh) and new silica-based thiol resin, which is similar to the published articles [53,73]. The detailed steps are as follows.

First, the sample solution containing 50–100 ng Sb was added to the 15 ml PFA beaker. 0.2 ml H_2O_2 (30%) and 0.6 ml HNO_3 (15.6 mol/L) were added to oxidize Sb(III) in the sample to Sb(V). Then the PFA beaker was opened and evaporated on a hot plate at 95 °C until the sample was almost dry (about 20 μl of liquid sample remaining). 1 ml 0.14 M HF was added to dissolve the sample, and then loaded onto the cation exchange resin column, and washed with 4 ml MQ water. The above 5 ml eluent containing Sb was received using PFA beaker, whereas matrix elements such as K, Ca, Fe, Zn, Pb, Ni, and Co would be retained on the ion exchange column. The recovery of Sb can reach 99%. This step can be repeated if the Fe content in the sample is too high. Second, the PFA beakers with eluent were placed on a hot plate at 95 °C until the sample was almost dry. 0.1 ml HCl (11.5 mol/L), 0.2 ml 10% (w/v) KI and L-ascorbic acid, and 0.7 ml MQ water were added to reduce Sb(V) in the solution to Sb(III). Before loading the sample solution onto the new silicon mercapto resin column, 1 ml MQ water was added to adjust the concentration of HCl of the sample solution to 0.5 M. Then residual matrix elements such as Fe, Cu, Zn and Sn in the previous step were eluted from the column with 5 ml 0.5 M HCl and 6 ml 2.5 M HCl. Finally, 5 ml 6 M HCl was added to wash Sb out of the column, and the eluent was collected in a PFA beaker. The recovery of Sb in this step can reach 100%. The Sb blank of the total experimental process is 0.3–0.5 ng, which accounts for only < 0.5% of the total sample load (100 ng).

The Sb isotopic composition of the samples was determined in low-resolution mode by a Nu plasma II MC-ICP—MS with a membrane desolvation (Aridus II) and a hydride generation system (HG) at the Institute of Geochemistry, Chinese Academy of Science [53,73]. The Sb concentration of the sample and standard solution was approximately 3 μg/L, corresponding to a signal intensity of approximately 1.5 v for ^{121}Sb. The instrument mass fractionation during Sb analysis was calibrated by the combination of standard-sample bracketing (SSB) and element doping method (ED). The long-term reproducibility of the instrument is $\delta^{123}Sb = 0.00 \pm 0.06‰$ (2 SD, N = 66) for NIST SRM 3102a (unprocessed) and $\delta^{123}Sb = 0.22 \pm 0.06‰$ (2 SD, N = 19) for Alfa Sb (unprocessed). After separation and purification, the $\delta^{123}Sb$ NIST SRM 3102a (processed) and $\delta^{123}Sb$ Alfa Sb (processed) values were 0.00 ± 0.06‰ (2 SD, N = 17) and 0.22 ± 0.06‰ (2 SD, N = 14), respectively. The $\delta^{123}Sb$ of the soil standard material 2711a was 0.21 ± 0.09‰ (2 SD, N = 17). Sb isotope data are expressed using the delta (δ) value as per mil deviation (‰) relative to the standard NIST SRM 3102a:

$$\delta 123Sb = \left[\frac{(123Sb/121Sb)_{sample}}{(123Sb/121Sb)_{\text{NIST SRM3102a}}} - 1\right] \times 1000 \quad (1)$$

The Sb isotopic compositions of geological and environmental reference materials (RMs) were also measured. The $\delta^{123}Sb$ values of the three stream sediment reference materials GSD-3, GSD-10 and GSD-11

were 0.46 ± 0.09‰ (2 SD, n = 6), 0.42 ± 0.12‰ (2 SD, n = 5), and 0.12 ± 0.11‰ (2 SD, n = 7), respectively. The δ^{123}Sb values of soil standard materials 2711a and GSS-5 were 0.23 ± 0.12‰ (2 SD, n = 7) and 0.32 ± 0.11‰ (2 SD, n = 7), respectively. The data of the above RMs are consistent with the published research [37,73]. It proves that all our experimental processes, including purification and isotope measurement, are reliable.

4. Results and discussion

4.1. Antimony concentration and TOC content

The concentration and trend of Sb in S1 and S2 are significantly different (Table 1). The Sb concentrations in S1 from the surface to the bottom are maintained at approximately 5 mg/kg, which is 2.2 times of the soil background value (2.24 mg/kg) of Guizhou Province [69]. This value is related to antimony mineralization and represents the geological background value of this area. Sb concentrations in S2 decrease exponentially from 74.60 mg/kg in the surface layer (0–10 cm) to 5.49 mg/kg in the bottom layer (50–80 cm). When below 50 cm, it returns to the geological background value and remains at approximately 5 mg/kg.

To further evaluate the losses and gains of Sb in the soil profiles, the relatively immobile element Zr was selected, and the normalized Sb concentrations in each soil layer relative to the reference layer were calculated [28] :

$$\tau_{Sb} = \frac{C_{Sb,hor} * C_{i,ref}}{C_{Sb,ref} * C_{i,hor}} - 1 \quad (2)$$

where $C_{Sb,hor}$ and $C_{Sb,ref}$, $C_{i,hor}$and $C_{i,ref}$are the concentrations of Sb and the reference element i in the reference horizon and the considered horizon, respectively. The positive and negative values of τ_{Sb} represent the gains and losses of Sb in the soil profile. The bottom layer was used as the reference layer, and the results are shown in Table 1 and Fig. 3.

The results indicate that the upper layers of both soil profiles exhibit accumulation relative to the bottom layers. The accumulation of Sb in S1 is low, the τ_{Sb} values range from 1.14 in the surface layer to 0 in the bottom layer, and the τ_{Sb} value at 10–20 cm is lower than that in the immediate upper and lower layers. The accumulation of Sb in S2 is high, and the τ_{Sb} values decrease from 14.8 in the surface layer to 0 in the bottom layer. According to the trend of normalized element concentrations in soil profiles, Brantley et al. divided soil profiles into 5 end-member categories [9]: immobile profiles, depletion profiles, depletion-enrichment profiles, addition profiles, and biogenic profiles. Element migration types of soil profiles may be produced by mixing one or several end-members. The τ_{Sb} values of S1 exhibit the characteristics of addition profiles, which may be related to surface runoff input or dry deposition of smelting source materials. However, according to the research of Xiong et al., the impact range of this smelter on the surrounding soil is less than 2 km [69]. Combined with the prevailing wind direction and the distance of S1 from the smelter, the impact of the smelting source on S1 can basically be excluded. In addition, S1 also has the characteristics of biogenic profiles. Plants extract Sb from pore water through the root system, along with the re-decomposition of plant litter, and then adsorption occurs in the surface layer, resulting in a lower τ_{Sb} value in the rhizosphere than in the adjacent upper and lower layers. The τ_{Sb} values of S2 exhibit the characteristics of addition profiles, which are influenced by the Sb input from the smelting source rather than natural weathering. In the soil below 50 cm, the τ_{Sb} values remain approximately 0, indicating that the migration ability of smelting source Sb in S2 is limited and mainly concentrated in the upper layer (0–50 cm).

The adsorption of organic matter is an important factor affecting the migration and transformation of Sb [24]. Previous studies have shown that Sb in soil is easily adsorbed by organic matter [16]. The analysis results of soil TOC show that the content and trend of TOC in the two profiles are significantly different, as shown in Table 1 and Fig. 3. The TOC content of S1 is low, and there is no significant variation within 0–80 cm. The TOC content of S2 is relatively high and shows a significant decreasing trend as a function of soil depth. Combined with the Sb concentration, the Sb content in the soil profile has a similar trend as the TOC content, indicating that the change of Sb content in soil may be related to the adsorption of organic matter.

Table 1
Selected chemical parameters and Sb isotopic composition of the soil profiles, plant and smelter-derived materials.

	Sb (mg/kg)	Zr (mg/kg)	τ_{Sb}[a]	Non-specifically sorbed Sb (mg/kg)	Specifically sorbed Sb (mg/kg)	TOC (%)	δ^{123}Sb (‰)	2 SD[b]
Contrasted Soils (S1)								
0–10 cm	6.19	336	1.14	0.0022	0.0136	0.27	0.49	0.09
10–20 cm	4.53	344	0.53	0.0030	0.0097	0.21	1.19	0.09
20–40 cm	5.38	389	0.61	0.0030	0.0114	0.24	1.19	0.09
40–60 cm	4.54	316	0.67	0.0003	0.0127	0.22	0.66	0.09
60–80 cm	4.10	476	0.00	0.0075	0.0233	0.61	0.59	0.09
Polluted Soils (S2)								
0–10 cm	74.60	247	14.75	0.3386	0.4292	2.33	0.28	0.09
10–25 cm	23.90	235	4.30	0.0886	0.6395	1.78	0.65	0.09
25–50 cm	10.70	238	1.34	0.0419	0.3116	1.72	0.27	0.09
50–80 cm	5.49	274	0.05	0.0091	0.0925	0.50	0.23	0.09
80–100 cm	5.10	266	0.00	0.0076	0.0455	0.33	0.58	0.09
Corn	0.87	nr[c]	nr	nr	nr	nr	0.03	0.09
Rice	1.86	nr	nr	nr	nr	nr	0.10	0.09
Antimony ore	2235	nr	nr	nr	nr	nr	0.30	0.09
Dust1	221287	nr	nr	nr	nr	nr	0.33	0.09
Dust2	646	nr	nr	nr	nr	nr	0.38	0.09
Slag	5116	nr	nr	nr	nr	nr	0.29	0.09
Smelter-derived materials	646–221287	nr	nr	nr	nr	nr	0.33 ± 0.08	-

[d]Mean value of the smelter-derived samples (antimony ore, slags, dust).
[a] Calculated according to Eq. (2).
[b] the SD of the soil standard material 2711a (0.21 ± 0.09‰, 2 SD, N = 17).
[c] Not relevant.

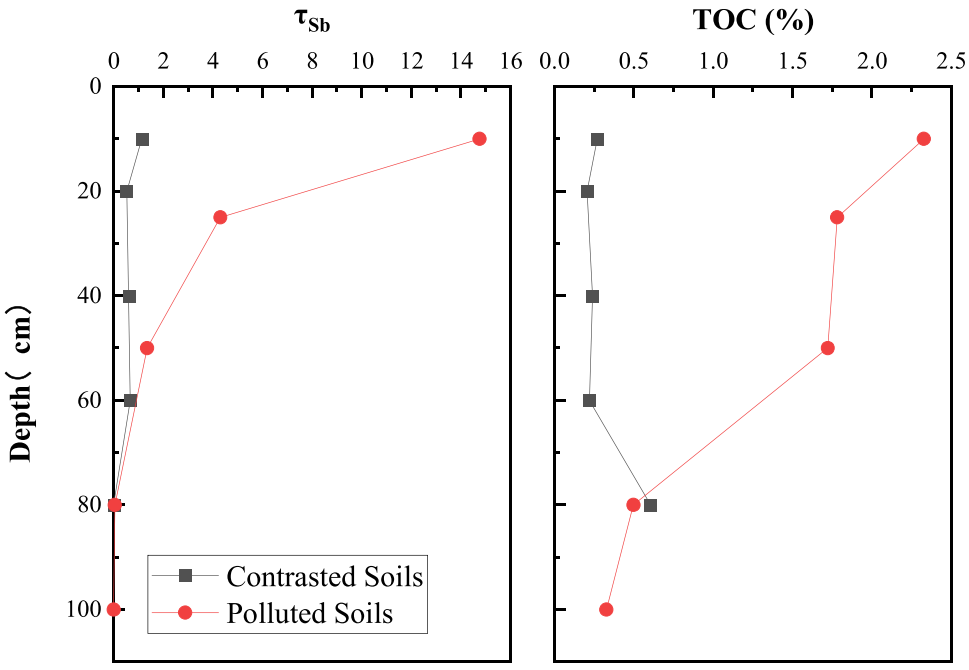

Fig. 3. Normalized Sb concentration and TOC content in contrasted and polluted soil profiles.

4.2. Easily migrated antimony

The SEPs results show that the proportion of non-specifically adsorbed Sb (F1) in S1 and S2 is close to zero, and the proportion of specifically adsorbed Sb (F2) is significantly different (Fig. 4). The proportion of F2 in S2 is relatively high, indicating a higher mobility of Sb. This difference may be related to the aging of Sb in those soils. Studies have shown that after adding Sb_2O_3 to the soil, 70% of the Sb will be oxidized to Sb^{5+} within two days. Sb^{5+}, as a more mobile form than Sb^{3+}, is more likely to migrate with pore water in the soil profile [34,46]. In addition, Diquattro monitored Sb in soil for up to 700 days and found that the content of easily migrated Sb gradually decreased over time due to the conversion of easily migrated Sb to the Fe/Al hydroxide phase [15]. Compared with the natural source Sb accumulated in the pedogenetic process, the time of smelting source Sb addition to the soil is shorter, and the migration ability is relatively higher. It can be inferred that the process of downwards migration of smelting source Sb mainly occurred in the initial stage of its deposition on the soil surface. Overall, the migration ability of Sb in the two profiles is limited, the proportion of easily migrated Sb is less than 4%, and the mobility of Sb

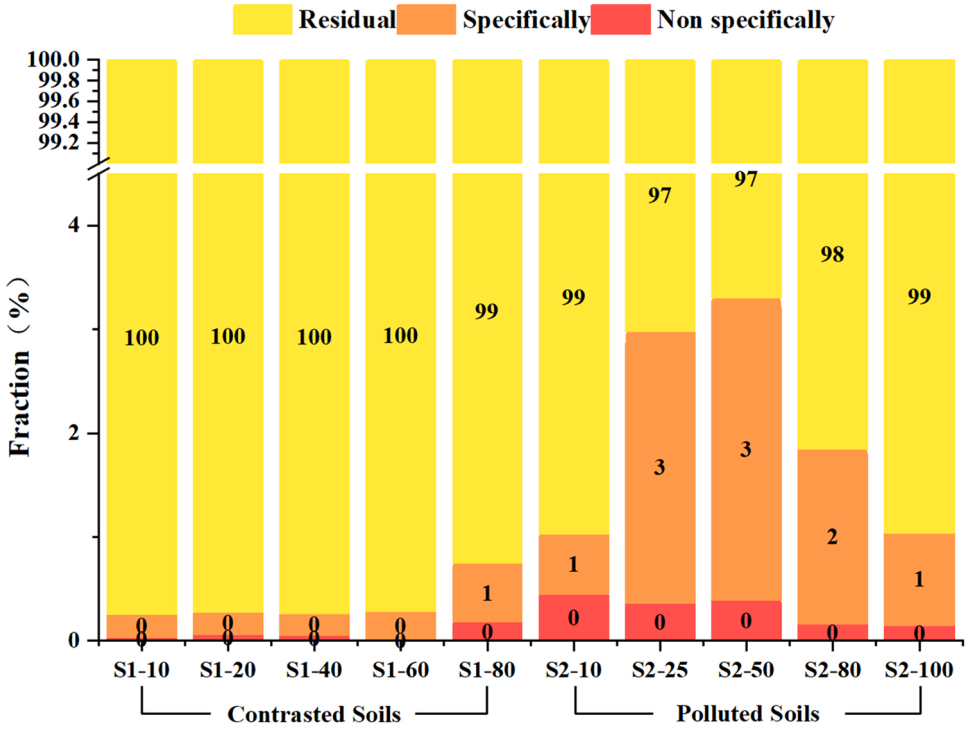

Fig. 4. Distribution of different Sb forms in the contrasted and polluted soil profiles.

in S2 is higher than that in S1.

4.3. 3.3 Isotopic composition of Sb from different sources

Sb isotope measurements were performed on plant samples, smelter-derived materials, and two soil profiles. The results are shown in Table 1 and Fig. 5.

The results show that the δ^{123}Sb value of the smelter-derived samples (antimony ore, slags, dust) varies in the range of 0.29–0.38‰ (mean value 0.29 ± 0.14‰), which can be defined as the Sb isotopic composition of the smelting source of this area. Sb isotopic compositions of the edible parts of rice and maize planted in this area are 0.03‰ and 0.10‰, respectively, which are the lightest Sb isotopic compositions in this batch of samples.

In S1, Sb isotope values of the 40–60 cm and 60–80 cm soils are 0.66‰ and 0.59‰, respectively, which are statistically similar. Therefore, the average Sb isotopic composition of the bottom layer of S1 is 0.63‰. Meanwhile, the Sb isotopic composition of the 80–100 cm soil in S2 is 0.58‰. It can be considered that the Sb isotopic composition in the deep layers of the two soil profiles is statistically similar and can be identified as the geogenic δ^{123}Sb value of the soil in this area. This result is consistent with the fact that the Sb in the deep layers of the two profiles originates from the same geological source. The geogenic δ^{123}Sb value in the deepest layer of the two soil profiles can be set as a mean value (0.61‰).

The δ^{123}Sb value of S1 at 0–10 cm is 0.49‰, which is slightly lower than the geogenic δ^{123}Sb value (0.61‰). The δ^{123}Sb values at 10–20 cm and 20–40 cm are similar, with an average value of 1.19‰, which is significantly heavier than the geogenic δ^{123}Sb value and is the heaviest Sb isotopic composition of this batch of samples. The δ^{123}Sb value of each layer of S2 is significantly lower than the Sb isotopic composition of the corresponding layer of S1. As mentioned in Section 3.1, the Sb in the upper layers of S2 is mainly derived from the smelting source. Compared with the δ^{123}Sb (0.33 ± 0.08‰) value of smelting source Sb, the δ^{123}Sb values of 0–10 cm (0.28‰) and 25–50 cm (0.27‰) are statistically similar, and the δ^{123}Sb value of 50–80 cm (0.23‰) is slightly lighter. Although the δ^{123}Sb value of 10–25 cm (0.65‰) is statistically similar to the geogenic δ^{123}Sb value, combined with the concentration of Sb, it should also be related to the mixing of smelter-derived materials.

4.4. Evidence for post-depositional modification of the δ^{123}Sb values

First, the δ^{123}Sb value of S1 is discussed, which would be helpful for further discussion of the cause of the δ^{123}Sb value in the upper layers of S2. The whole soil profile of S1 should have a geogenic δ^{123}Sb value (0.61‰) similar to that of the bottom soil if no other post-depositional modification processes resulted in the fractionation of Sb isotopes. However, the δ^{123}Sb values of S1 at 0–40 cm are not the same as the geogenic δ^{123}Sb value. As mentioned in Section 3.1, the surface layer 0–10 cm of S1 may be affected by the addition of Sb from the smelting source. Through mass balance calculation (Eq. 3), combined with the geological Sb background value (5 mg/kg), the assumed δ^{123}Sb value of 0–10 cm soil after mixing is 0.56‰, which can be considered to be statistically similar to the measured δ^{123}Sb value (0.49‰) of 0–10 cm soil. However, although it can explain the Sb isotopic composition of the 0–10 cm soil, it cannot explain the enrichment of the heavy isotope in 10–40 cm of S1. As mentioned in 3.1, the SEPs results show that the migration ability of Sb in S1 is limited. The variation of the δ^{123}Sb value cannot be caused by the downwards migration of Sb. Therefore, the influence of the addition of smelting source Sb on 10–40 cm of S1 can be excluded. The δ^{123}Sb value should be affected by other post-depositional modification processes.

$$\delta T = \frac{\delta_A C_A + \delta_B C_B}{C_T} \quad (3)$$

where δ and C represent the Sb isotopic composition and the concentration of Sb, respectively. A and B represent different endmembers, and T represents the total sample after mixing. It is assumed that the total volume of the soil does not change significantly after mixing each endmember.

As mentioned in Section 3.1, most of the Sb in the upper part of S2 is related to the addition of Sb from the smelting source. To further discuss the variation in Sb isotopic fractionation caused by the migration of smelting source Sb in S2, it is assumed that the natural source Sb in the two soil profiles has undergone the same biogeochemical process and has similar antimony isotopic composition and distribution characteristics in both soil profiles. Therefore, the difference in the δ^{123}Sb values of different layers between S1 and S2 is mainly caused by the addition and migration of Sb from the smelting source in S2. According to the mass balance calculation (Eq. 3), combined with the Sb concentration data of different layers, the Sb isotopic compositions of the addition part from the smelting source at 0–10 cm, 10–25 cm, 25–50 cm, and 50–80 cm of S2 are 0.26‰, 0.49‰, −0.01‰ and −0.85‰, respectively, as shown by the blue line (Fig. 6). Compared with the δ^{123}Sb value of

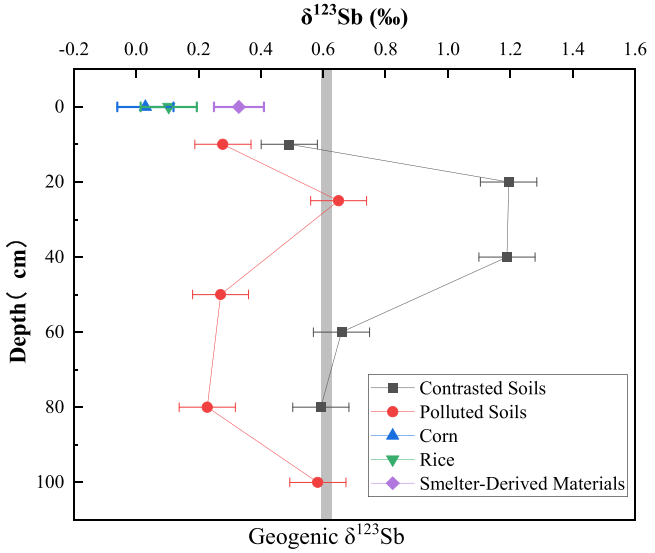

Fig. 5. Isotopic composition of Sb from different sources and two soil profiles.

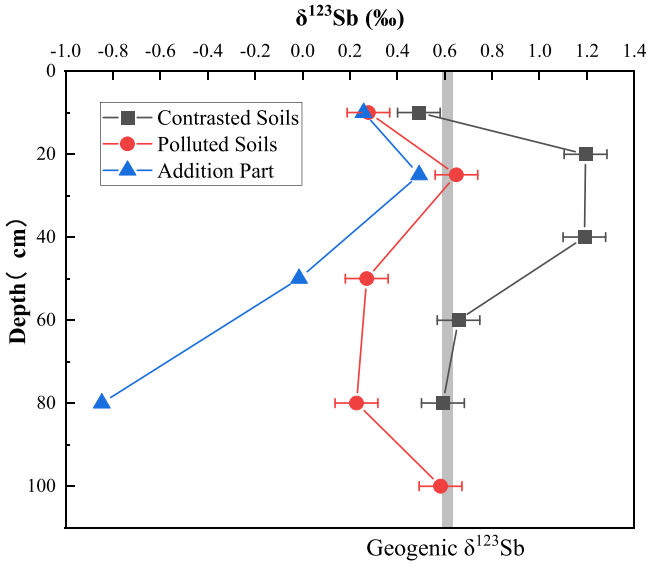

Fig. 6. Antimony isotopic composition of the addition part of the smelting source in the soil profile.

smelting source Sb (0.33 ± 0.08‰), the δ^{123}Sb values of 0–10 cm, 10–25 cm, and 25–80 cm soils show differences of lighter, heavier, and lighter, respectively. This indicates that the smelting source of Sb is affected by other biogeochemical processes during its downwards migration after deposition on the soil surface, and the upper and bottom layers are controlled by different biogeochemical processes, leading to the loss of heavy isotopes at 0–10 cm, enrichment of heavy isotopes at 10–25 cm, and enrichment of light isotopes at 25–80 cm.

4.5. Biogeochemical processes possibly responsible for the isotope fractionation of antimony

The adsorption process is the most important natural process controlling the migration and transformation of Sb in soil systems [7,25]. Sb can be adsorbed by different soil components, including metal (hydro) oxides, clay minerals, and organic matter. Studies have shown that heavy isotopes are often enriched in metal-organic complexes compared with free aqueous ones due to the relatively strong bonding environment [66]. As mentioned in Section 3.2, the variation in Sb content in the soil profile may be related to the adsorption of organic matter. However, combined with the antimony isotopic composition of the soil profile, the trend of δ^{123}Sb value is not correlated with the trend of TOC content, indicating that the adsorption of organic matter has a negligible effect on the isotopic composition of Sb in the soil profile.

Antimony often exists in the form of anionic metal species in soil pore water, and the adsorption of anionic metal species usually results in the enrichment of heavy isotopes in the liquid phase [66,68]. Araki et al. also showed that the adsorption of Sb^{5+} by synthetic ferrihydrite resulted in the enrichment of heavy isotopes in the liquid phase [2]. Therefore, heavy antimony isotopes may be enriched in the pore water of the soil profile, and downwards migration of the pore water will lead to a heavier isotopic composition in the lower layer. It can be used to explain the enrichment of heavy isotopes in the 10–40 cm layer of S1. However, combined with the Sb concentration data of the soil profile, the Sb concentration in the surface layer of S1 is higher than that in the lower layer. Enrichment of heavy antimony isotopes at 10–40 cm could not be explained solely by the downwards migration of the pore water. Therefore, the enrichment of heavy isotopes should be related to other biogeochemical processes in addition to the adsorption process.

Based on the Sb concentration data of S1, the τ_{Sb} value of S1 is characteristic of the biogenic profile. Although there have been many studies on the uptake and transport process of Sb in plants, there is no report on the fractionation of Sb isotopes in this process [43,75]. Studies on the fractionation of stable isotopes of other metals in the process showed that most of the isotopes were enriched in light isotopes, except for Mg isotopes in plants [66]. The two plant samples have the lightest antimony isotopic composition (0.03‰ and 0.10‰) of the samples measured in this batch of experiments. It is suggested that, similar to most elements, plants preferentially take up and transport light Sb isotopes in soil—plant systems, resulting in a heavier Sb isotopic composition in the rhizosphere soil. Roots of annual herbaceous plants are mainly distributed in the 0–40 cm range [17], which explains the heavy isotope enrichment measured in the 10–40 cm layer of S1. Meanwhile, the light δ^{123}Sb value in the 0–10 cm layer of S1 could be explained by the adsorption of light Sb isotopes from the decomposition of plant litter. However, Sb is not an essential element for plant growth and the average accumulation factor of Sb by plants is only 0.02 [57], so the uptake ability of Sb by plants is limited. It takes a long time and repeated uptake process to affect the Sb isotopic composition of the rhizosphere soil. Therefore, this process may be the main factor controlling the variation in Sb isotopic composition in S1, while it has less effect on the Sb isotopic composition of S2.

The variation in Sb isotopic composition in S2 is mainly related to the addition of Sb from the smelting source. According to the SEPs and Sb concentration results, at the beginning of the smelting source Sb entering the soil, a large part of Sb may dissolve into the pore water and then migrate downwards and adsorb in the lower layer. Loss and enrichment of heavy antimony isotopes in the 0–10 cm and 10–25 cm soil layers may be related to the leaching of pore water enriched in heavy antimony isotopes and adsorption in the lower layer. However, enrichment of light antimony isotopes in 25–80 cm soil is difficult to explain by the processes described above. Previous studies have shown that light antimony isotopes are enriched in the reduced phase during the reduction of Sb^{5+} [49]. Meanwhile, reduction and dissolution of iron (hydro)oxide will lead to the release of Sb into pore water in the form of Sb^{3+} [26], which may lead to the enrichment of light antimony isotopes in pore water. Due to the change in redox conditions in the soil profile, the reductive dissolution process is likely to occur in the lower layer of S2, which could explain the gradually lighter antimony isotope composition in the 25–80 cm soil.

In addition to the above possible processes, other biogeochemical processes (precipitation-dissolution, microbial methylation, etc.) may also affects the isotopic composition of Sb in the soil profile. At present, the theoretical system of antimony isotope fractionation is incomplete, the data on antimony isotopes in soil systems and related studies are scarce, and whether the interpretation of the data is universal still needs more experimental data for support, such as spectroscopic techniques (EXAFS) and more representative sampling methods. It will be a promising research field to further understand and reveal the migration and transformation behaviors of Sb in soil profiles through antimony isotope data in combination with the existing valence state, binding state, and distribution ratio of Sb in soil [31,66].

5. Conclusion

In this paper, the variation of antimony isotopes in the soil profile and their possible fractionation mechanism is studied for the first time, which provides theoretical support and basic data for tracing the migration and transformation of Sb in soil. The results show that distinct fractionation of Sb isotopes occurred in the soil profile, which, combined with the SEPs results, could reveal and deepen the understanding of the migration and transformation process of Sb in the soil. The main conclusions are as follows: 1) The migration ability of Sb from the smelting source is stronger than that from the natural source; 2) isotope fractionation of the natural source Sb may be controlled by the plant uptake process; and 3) isotopic fractionation of the smelting source Sb in the surface and bottom layers may be controlled by absorption and reductive dissolution, respectively. Further study on the mechanism of Sb isotope fractionation, verification, and determination of the fractionation direction and magnitude of Sb isotopes in different biogeochemical processes will play a crucial role in understanding the migration and transformation behaviors of Sb in environmental media.

CRediT authorship contribution statement

Jie Liao: Investigation, Data curation, Validation, Formal analysis, Visualization, Writing - original draft, Writing - review & editing. **Decan Tan:** Resources, Formal analysis, Review & editing, Visualization, Methodology, Writing - review & editing. **Haibo Qin** and **Qiao Han:** Writing - review & editing. **Enguang Liu:** Data curation. **Jingan Chen:** Resources, Project administration. **Zengping Ning** and **Shehong Li:** Resources, Writing - review & editing, Conceptualization, Project administration, Supervision.

Declaration of Competing Interest

The authors declare that they have no known competing financial interests or personal relationships that could have appeared to influence the work reported in this paper.

Data availability

Data will be made available on request.

Acknowledgements

This work was supported by Strategic Priority Research Program of Chinese Academy of Sciences (No. XDB40000000), the United Fund of the Guizhou Province Government and Natural Science Foundation of China (No. U1612442), the National Natural Science Foundation of China (No. 42177182), and the Central Government leading local science and technology development (QianKeZhongYinDi [2021]4028).

References

[1] Ainsworth, N., Cooke, J.A., Johnson, M.S., 1990. Distribution of antimony in contaminated grassland.1. vegetation and soils [J]. Environ Pollut 65, 65–77. https://doi.org/10.1016/0269-7491(90)90165-9.
[2] Araki, Y., Tanimizu, M., Takahashi, Y., 2009. Antimony isotopic fractionation during adsorption on ferrihydrite [J]. Geochim Et Cosmochim Acta Suppl 73, A49.
[3] Asaoka, S., Takahashi, Y., Araki, Y., et al., 2011. Preconcentration method of antimony using modified thiol cotton fiber for isotopic analyses of antimony in natural samples [J]. Anal Sci 27, 25–28. https://doi.org/10.2116/analsci.27.25.
[4] Berglund, M., Wieser, M.E., 2011. Isotopic compositions of the elements 2009 (IUPAC Technical Report) [J]. Pure Appl Chem 83, 397–410. https://doi.org/10.1351/PAC-REP-10-06-02.
[5] Beyersmann, D., Hartwig, A., 2008. Carcinogenic metal compounds: recent insight into molecular and cellular mechanisms [J]. Arch Toxicol 82, 493–512. https://doi.org/10.1007/s00204-008-0313-y.
[6] Bigalke, M., Weyer, S., Kobza, J., et al., 2010. Stable Cu and Zn isotope ratios as tracers of sources and transport of Cu and Zn in contaminated soil [J]. Geochim Et Cosmochim Acta 74, 6801–6813. https://doi.org/10.1016/j.gca.2010.08.044.
[7] Bolan, N., Kumar, M., Singh, E., et al., 2022. Antimony contamination and its risk management in complex environmental settings: a review [J]. Environ Int 158, 106908. https://doi.org/10.1016/j.envint.2021.106908.
[8] Boreiko, C.J., Rossman, T.G., 2020. Antimony and its compounds: health impacts related to pulmonary toxicity cancer and genotoxicity [J]. Toxicol Appl Pharmacol 403, 115156. https://doi.org/10.1016/j.taap.2020.115156.
[9] Brantley, S.L., Goldhaber, M.B., Ragnarsdottir, K.V., 2007. Crossing disciplines and scales to understand the Critical Zone [J]. Elements 3, 307–314. https://doi.org/10.2113/gselements.3.5.307.
[10] Burton, E.D., Hockmann, K., Karimian, N., 2020. Antimony sorption to goethite: effects of Fe(II)-Catalyzed recrystallization [J]. Acs Earth Space Chem 4, 476–487. https://doi.org/10.1021/acsearthspacechem.0c00013.
[11] Chang, Y., Zhang, J., Qu, J.Q., et al., 2017. Precise selenium isotope measurement in seawater by carbon-containing hydride generation-desolvation-MC-ICP-MS after thiol resin preconcentration [J]. Chem Geol 471, 65–73. https://doi.org/10.1016/j.chemgeo.2017.09.011.
[12] Cloquet, C., Carignan, J., Libourel, G., et al., 2006. Tracing source pollution in soils using cadmium and lead isotopes [J]. Environ Sci Technol 40, 2525–2530. https://doi.org/10.1021/es052232+.
[13] Degryse, P., Lobo, L., Shortand, A., et al., 2015. Isotopic investigation into the raw materials of Late Bronze Age glass making [J]. J Archaeol Sci 62, 153–160. https://doi.org/10.1016/j.jas.2015.08.004.
[14] Dillis, S., Van Ham-Meert, A., Leeming, P., et al., 2019. Antimony as a raw material in ancient metal and glass making: provenancing Georgian LBA metallic Sb by isotope analysis, 5. Science & Technology of Archaeological Research [J],, STAR, pp. 98–112. https://doi.org/10.1080/20548923.2019.1681138.
[15] Diquattro, S., Castaldi, P., Ritch, S., et al., 2021. Insights into the fate of antimony (Sb) in contaminated soils: ageing influence on Sb mobility bioavailability bioaccessibility and speciation [J]. Sci Total Environ 770, 145354. https://doi.org/10.1016/j.scitotenv.2021.145354.
[16] Dousova, B., Buzek, F., Herzogova, L., et al., 2015. Effect of organic matter on arsenic(V) and antimony(V) adsorption in soils [J]. Eur J Soil Sci 66, 74–82. https://doi.org/10.1111/ejss.12206.
[17] Feng, H.B., Zhou, J.W., Zhou, A.G., et al., 2021. Grassland ecological restoration based on the relationship between vegetation and its below-ground habitat analysis in steppe coal mine area [J]. Sci Total Environ 778, 146221. https://doi.org/10.1016/j.scitotenv.2021.146221.
[18] Ferrari, C., Meheut, M., Resongles, E., et al., 2022. Equilibrium mass-dependent isotope fractionation of antimony between stibnite and Sb secondary minerals: a first-principles study [J]. Chem Geol 611, 121115. https://doi.org/10.1016/j.chemgeo.2022.121115.
[19] Filella, M., 2011. Antimony interactions with heterogeneous complexants in waters, sediments and soils: a review of data obtained in bulk samples [J]. Earth-Sci Rev 107, 325–341. https://doi.org/10.1016/j.earscirev.2011.04.002.
[20] Filella, M., Belzile, N., Chen, Y.-W., 2002. Antimony in the environment: a review focused on natural waters: i. occurrence [J]. Earth-Sci Rev 57, 125–176. https://doi.org/10.1016/S0012-8252(01)00070-8.
[21] Filella, M., Williams, P.A., Belzile, N., 2009. Antimony in the environment: knowns and unknowns [J]. Environ Chem 6, 95–105. https://doi.org/10.1071/EN09007.
[22] Hansell, C., 2015. All manner of antimony [J], 88-88 Nat Chem 7. https://doi.org/10.1038/nchem.2134.
[23] He, M., Wang, X., Wu, F., et al., 2012. Antimony pollution in China [J]. Sci Total Environ 421–422, 41–50. https://doi.org/10.1016/j.scitotenv.2011.06.009.
[24] He, M.C., Wang, N.N., Long, X.J., et al., 2019. Antimony speciation in the environment: recent advances in understanding the biogeochemical processes and ecological effects [J]. J Environ Sci 75, 14–39. https://doi.org/10.1016/j.jes.2018.05.023.
[25] Herath, I., Vithanage, M., Bundschuh, J., 2017. Antimony as a global dilemma: geochemistry mobility fate and transport [J]. Environ Pollut 223, 545–559. https://doi.org/10.1016/j.envpol.2017.01.057.
[26] Hockmann, K., Lenz, M., Tandy, S., et al., 2014. Release of antimony from contaminated soil induced by redox changes [J]. J Hazard Mater 275, 215–221. https://doi.org/10.1016/j.jhazmat.2014.04.065.
[27] Howarth, S., Prytulak, J., Little, S.H., et al., 2018. Thallium concentration and thallium isotope composition of lateritic terrains [J]. Geochim Et Cosmochim Acta 239, 446–462. https://doi.org/10.1016/j.gca.2018.04.017.
[28] Juillot, F., Marechal, C., Morin, G., et al., 2011. Contrasting isotopic signatures between anthropogenic and geogenic Zn and evidence for post-depositional fractionation processes in smelter-impacted soils from Northern France [J]. Geochim Et Cosmochim Acta 75, 2295–2308. https://doi.org/10.1016/j.gca.2011.02.004.
[29] Karimian, N., Johnston, S.G., Burton, E.D., 2017. Antimony and Arsenic behavior during Fe(II)-Induced transformation of jarosite [J]. Environ Sci Technol 51, 4259–4268. https://doi.org/10.1021/acs.est.6b05335.
[30] Kersten, M., Xiao, T.F., Kreissig, K., et al., 2014. Tracing anthropogenic thallium in soil using stable isotope compositions [J]. Environ Sci Technol 48, 9030–9036. https://doi.org/10.1021/es501968d.
[31] Komarek, M., Ratie, G., Vankova, Z., et al., 2022. Metal isotope complexation with environmentally relevant surfaces: opening the isotope fractionation black box [J]. Crit Rev Environ Sci Technol 52, 3573–3603. https://doi.org/10.1080/10643389.2021.1955601.
[32] Krachler, M., Zheng, J., Koerner, R., et al., 2005. Increasing atmospheric antimony contamination in the northern hemisphere: snow and ice evidence from Devon Island Arctic Canada [J]. J Environ Monit 7, 1169–1176. https://doi.org/10.1039/b509373b.
[33] Lei, H.W., Chen, J.J., Tan, Z.J., et al., 2019. Review of recent progress in antimony chalcogenide-based solar cells: materials and devices [J]. Sol Rrl 3, 1900026. https://doi.org/10.1002/solr.201900026.
[34] Leuz, A.K., Monch, H., Johnson, C.A., 2006. Sorption of Sb(III) and Sb(V) to goethite: influence on Sb(III) oxidation and mobilization [J]. Environ Sci Technol 40, 7277–7282. https://doi.org/10.1021/es061284b.
[35] Li, S., Deng, Y., Zheng, H., et al., 2021. A new purification method based on a thiol silica column for high precision antimony isotope measurements [J]. J Anal Spectrom 36, 157–164. https://doi.org/10.1039/d0ja00367k.
[36] Liang, Q., Jing, H., Gregoire, D.C., 2000. Determination of trace elements in granites by inductively coupled plasma mass spectrometry [J]. Talanta 51, 507–513. https://doi.org/10.1016/s0039-9140(99)00318-5.
[37] Liu, J.F., Chen, J.B., Zhang, T., et al., 2020. Chromatographic purification of antimony for accurate isotope analysis by MC-ICP-MS [J]. J Anal Spectrom 35, 1360–1367. https://doi.org/10.1039/d0ja00136h.
[38] Lobo, L., Degryse, P., Shortland, A., et al., 2014. Copper and antimony isotopic analysis via multi-collector ICP-mass spectrometry for provenancing ancient glass [J]. J Anal Spectrom 29, 58–64. https://doi.org/10.1039/c3ja50303h.
[39] Lobo, L., Degryse, P., Shortland, A., et al., 2013. Isotopic analysis of antimony using multi-collector ICP-mass spectrometry for provenance determination of Roman glass [J]. J Anal Spectrom 28, 1213–1219. https://doi.org/10.1039/c3ja50018g.
[40] Lobo, L., Devulder, V., Degryse, P., et al., 2012. Investigation of natural isotopic variation of Sb in stibnite ores via multi-collector ICP-mass spectrometry - perspectives for Sb isotopic analysis of Roman glass [J]. J Anal Spectrom 27, 1304–1310. https://doi.org/10.1039/c2ja30062a.
[41] Luo, Y., Huang, Z., Xiao, X., et al., 2014. Contents of ore-forming elements and geological significance of dushan antimony ore field Guizhou Province China [J]. Acta Mineral Sin 34, 247–253. https://doi.org/10.16461/j.cnki.1000-4734.2014.02.015.
[42] Mitsunobu, S., Harada, T., Takahashi, Y., 2006. Comparison of antimony behavior with that of arsenic under various soil redox conditions [J]. Environ Sci Technol 40, 7270–7276. https://doi.org/10.1021/es060694x.
[43] Natasha, Shahid, M., Khalid, S., et al., 2019. Biogeochemistry of antimony in soil-plant system: ecotoxicology and human health [J]. Appl Geochem 106, 45–59. https://doi.org/10.1016/j.apgeochem.2019.04.006.
[44] Ngo, L.K., Price, H.L., Bennett, W.W., et al., 2020. DGT and selective extractions reveal differences in arsenic and antimony uptake by the white icicle radish (Raphanus sativus) [J]. Environ Pollut 259, 113815. https://doi.org/10.1016/j.envpol.2019.113815.
[45] Ning, Z.P., Xiao, T.F., Xiao, E.Z., 2015. Antimony in the soil-plant system in an Sb mining/smelting area of Southwest China [J]. Int J Phytoremediat 17, 1081–1089. https://doi.org/10.1080/15226514.2015.1021955.
[46] Oorts, K., Smolders, E., Degryse, F., et al., 2008. Solubility and toxicity of antimony trioxide (Sb2O3) in soil [J]. Environ Sci Technol 42, 4378–4383. https://doi.org/10.1021/es703061t.
[47] Park, S.C., Boyanov, M.I., Kemner, K.M., et al., 2021. Distribution and speciation of Sb and toxic metal(loid)s near an antimony refinery and their effects on indigenous microorganisms [J]. J Hazard Mater 403, 123625. https://doi.org/10.1016/j.jhazmat.2020.123625.

[48] Resongles, E., Freydier, R., Casiot, C., et al., 2015. Antimony isotopic composition in river waters affected by ancient mining activity [J]. Talanta 144, 851–861. https://doi.org/10.1016/j.talanta.2015.07.013.
[49] Rouxel, O., Ludden, J., Fouquet, Y., 2003. Antimony isotope variations in natural systems and implications for their use as geochemical tracers [J]. Chem Geol 200, 25–40. https://doi.org/10.1016/S0009-2541(03)00121-9.
[50] Shotyk, W., Krachler, M., Chen, B., 2005. Antimony: global environmental contaminant [J]. J Environ Monit 7, 1135–1136. https://doi.org/10.1039/b515468p.
[51] Singh, Y., Maurya, K.K., Singh, V.N., et al., 2021. A review on properties applications and deposition techniques of antimony selenide [J]. Sol Energy Mater Sol Cells 230, 111223. https://doi.org/10.1016/j.solmat.2021.111223.
[52] Sivry, Y., Riotte, J., Sonke, J.E., et al., 2008. Zn isotopes as tracers of anthropogenic pollution from Zn-ore smelters the Riou Mort-Lot river system [J]. Chem Geol 255, 295–304. https://doi.org/10.1016/j.chemgeo.2008.06.038.
[53] Sun, G.Y., Wu, Y.J., Feng, X.B., et al., 2021. Precise analysis of antimony isotopic composition in geochemical materials by MC-ICP-MS [J]. Chem Geol 582, 120459. https://doi.org/10.1016/j.chemgeo.2021.120459.
[54] Tan, D.C., Zhu, J.M., Wang, X.L., et al., 2020. High-sensitivity determination of Cd isotopes in low-Cd geological samples by double spike MC-ICP-MS [J]. J Anal Spectrom 35, 713–727. https://doi.org/10.1039/c9ja00397e.
[55] Tanimizu, M., Araki, Y., Asaka, S., et al., 2011. Determination of natural isotopic variation in antimony using inductively coupled plasma mass spectrometry for an uncertainty estimation of the standard atomic weight of antimony [J]. Geochem J 45, 27–32. https://doi.org/10.2343/geochemj.1.0088.
[56] Tighe, M., Lockwood, P., 2007. Importance of noncrystalline hydroxide phases in sequential extractions to fractionate antimony in acid soils [J]. Commun Soil Sci Plant Anal 38, 1487–1501. https://doi.org/10.1080/00103620701378441.
[57] Tschan, M., Robinson, B.H., Schulin, R., 2009. Antimony in the soil-plant system - a review [J]. Environ Chem 6, 106–115. https://doi.org/10.1071/en08111.
[58] Ullrich, M.K., Pope, J.G., Seward, T.M., et al., 2013. Sulfur redox chemistry governs diurnal antimony and arsenic cycles at champagne pool waiotapu New Zealand [J]. J Volcanol Geotherm Res 262, 164–177. https://doi.org/10.1016/j.jvolgeores.2013.07.007.
[59] Wang, D., Mathur, R., Zheng, Y.Y., et al., 2021. Redox-controlled antimony isotope fractionation in the epithermal system: new insights from a multiple metal stable isotopic combination study of the Zhaxikang Sb-Pb-Zn-Ag deposit in Southern Tibet [J]. Chem Geol 584. https://doi.org/10.1016/j.chemgeo.2021.120541.
[60] Wang, Q., Ren, Y., Meng, L., et al., 2013. Simultaneous determination of total nitrogen and organic carbon in soil with an elemental analyzer [J]. Chin J Anal Lab 32, 41–45. https://doi.org/10.13595/j.cnki.issn1000-0720.2013.0265.
[61] Wang, R.R., Yu, H.M., Cheng, W.H., et al., 2022. Copper migration and isotope fractionation in a typical paddy soil profile of the Yangtze Delta [J]. Sci Total Environ 821, 153201. https://doi.org/10.1016/j.scitotenv.2022.153201.
[62] Wehmeier, S., Ellam, R., Feldmann, J., 2003. Isotope ratio determination of antimony from the transient signal of trimethylstibine by GC-MC-ICP-MS and GC-ICP-TOF-MS [J]. J Anal Spectrom 18, 1001–1007. https://doi.org/10.1039/b302242k.
[63] Weiss, D.J., Rehkaemper, M., Schoenberg, R., et al., 2008. Application of nontraditional stable-isotope systems to the study of sources and fate of metals in the environment [J]. Environ Sci Technol 42, 655–664. https://doi.org/10.1021/es0870855.
[64] Wen, B., Zhou, J.W., Zhou, A.G., et al., 2018. A review of antimony (Sb) isotopes analytical methods and application in environmental systems [J]. Int Biodeterior Biodegrad 128, 109–116. https://doi.org/10.1016/j.ibiod.2017.01.008.
[65] Wenzel, W.W., Kirchbaumer, N., Prohaska, T., et al., 2001. Arsenic fractionation in soils using an improved sequential extraction procedure [J]. Anal Chim Acta 436, 309–323. https://doi.org/10.1016/S0003-2670(01)00924-2.
[66] Wiederhold, J.G., 2015. Metal stable isotope signatures as tracers in environmental geochemistry [J]. Environ Sci Technol 49, 2606–2624. https://doi.org/10.1021/es504683e.
[67] Wiederhold, J.G., Teutsch, N., Kraemer, S.M., et al., 2007. Iron isotope fractionation during pedogenesis in redoximorphic soils [J]. Soil Sci Soc Am J 71, 1840–1850. https://doi.org/10.2136/sssaj2006.0379.
[68] Wilson, S.C., Lockwood, P.V., Ashley, P.M., et al., 2010. The chemistry and behaviour of antimony in the soil environment with comparisons to arsenic: a critical review [J]. Environ Pollut 158, 1169–1181. https://doi.org/10.1016/j.envpol.2009.10.045.
[69] Xiong, J., Han, Z., Wu, P., et al., 2020. Spatial distribution characteristics contamination evaluation and health risk assessment of arsenic and antimony in soil around an antimony smelter of Dushan County [J]. Acta Sci Circumstantiae 40, 655–664. https://doi.org/10.13671/j.hjkxxb.2019.0387.
[70] Yin, Y.W., Jiang, C.H., Ma, Y.Y., et al., 2021. Sequential coevaporation and deposition of antimony selenosulfide thin film for efficient solar cells [J]. Adv Mater 33, 2006689. https://doi.org/10.1002/adma.202006689.
[71] You, X.M., Xiao, Y., Liu, K., et al., 2020. Association of plasma antimony concentration with markers of liver function in Chinese adults [J]. Environ Chem 17, 304–313. https://doi.org/10.1071/en19195.
[72] Zhai, D., Mathur, R., Liu, S.-A., et al., 2021. Antimony isotope fractionation in hydrothermal systems [J]. Geochim Et Cosmochim Acta 306, 84–97. https://doi.org/10.1016/j.gca.2021.05.031.
[73] Zhao, B., Zhu, J., Qin, H., et al., 2018. Research progress in measurement and application of antimony isotope [J]. Bull Mineral Petrol Geochem 37, 1181–1189. https://doi.org/10.19658/j.issn.1007-2802.2018.37.058.
[74] Zhu, J.M., Wu, G.L., Wang, X.L., et al., 2018. An improved method of Cr purification for high precision measurement of Cr isotopes by double spike MC-ICP-MS [J]. J Anal Spectrom 33, 809–821. https://doi.org/10.1039/c8ja00033f.
[75] Zhu, Y.M., Yang, J.G., Wang, L.Z., et al., 2020. Factors influencing the uptake and speciation transformation of antimony in the soil-plant system, and the redistribution and toxicity of antimony in plants [J]. Sci Total Environ 738, 140232. https://doi.org/10.1016/j.scitotenv.2020.140232.